The coupled-cluster Monte Carlo method on the uniform electron gas

Blind Candidate Number: 2020C

Cavendish Laboratory, Department of Physics, J J Thomson Avenue, Cambridge. CB3 0HE

Abstract

In this work, the coupled-cluster Monte Carlo (CCMC) method was used to perform benchmark-level calculations on the uniform electron gas (UEG) systems of r_s ranging from 0.1 to 10, with electron numbers of up to 54, up to CCSDTQ truncation level. The effect of the new quasi-Newton propagation algorithm on the computational cost of the method was also studied, in addition to those of the timestep, the initial population, and the excitation generator. It was found that the timestep had the largest effect on the computational cost, followed by the even selection algorithm; whilst other parameters generally affected the stochastic noise. Additionally, an implementation of the Davidson-Liu algorithm for approxmiate full configuration interaction (FCI) calculations in the HANDE-QMC pacakge was reported and tested on UEG and molecular systems, with excellent agreements with FCI obtained for all systems.

Contents

1. Introduction

Quantum Monte Carlo (QMC) methods are a class of post-mean-field methods that integrates over the phase space using stochastic algorithms in contrast to the exact numerical integration in deterministic, or classical electronic structure methods.

Almost all of the QMC methods start with the *projector method*, based on the *time-dependent Schrödinger equation*:

$$i\frac{\partial\Psi}{\partial t} = \hat{\mathbf{H}}\Psi \tag{1}$$

A Wick rotation ($it \rightarrow \tau$) gives the *imaginary-time Schrödinger equation*:

$$\frac{\partial\Psi}{\partial\tau} = -\hat{\mathbf{H}}\Psi \tag{2}$$

which can be formally integrated to give:

$$\Psi(\tau) = \exp(-\tau(\hat{\mathbf{H}} - S))\Psi(0) \tag{3}$$

This can be regarded as the 'master equation' for the projector methods. The constant of integration, S, is also known as the arbitrary 'shift' parameter.

QMC methods generally suffer from the fermion sign problem [1], which is the incompatibility of the Monte Carlo algorithm which represents a fermionic wavefunction Ψ as a collection of walkers with positive and negative weights, and the interpretation of $|\Psi|^2$ as a probability distribution function, meaning that most random-walk paths will eventually suffer from numerical cancel-

lation, leaving the real contributions exponentially small as the algorithm progresses [2, p. 15.14].

At this point, the field diverges along the choice of the form of Ψ, into broadly two categories:

- **Real-space QMC** methods use real-space, continuous functions for Ψ. These include variational Monte Carlo (VMC) and diffusion Monte Carlo (DMC), where the former is now commonly used to prepare trial wavefunctions for the latter. For a recent review on the state-of-the art of these methods, see [3]. DMC generally ameliorate the sign problem by imposing the *fixed-node approximation* [4, 5], which imposes an infinite repulsive potential at nodal (hyper-)surfaces of a wavefunction of the same system taken from a cheaper theory, with Hartree-Fock (HF) and Kohn-Sham density functional theory (KS-DFT) being commonly used.

- **Fock-space QMC** methods use linear combinations of Slater determinants for Ψ. These include the auxiliary-field quantum Monte Carlo (AFQMC) [6], full configuration-interaction quantum Monte Carlo (FCIQMC) [7], coupled-cluster Monte Carlo (CCMC) [8] and density matrix quantum Monte Carlo (DMQMC) [9]. As Slater determinants are anti-symmetrised, there is no problem of converging to a bosonic solution, as can happen in DMC, and this reduces the severity of the sign problem somewhat. AFQMC stands in its own sub-class, and suppresses the sign problem with the *phaseless approximation*. The remaining methods belongs to a family of related algorithms, where the sign problem is addressed elegantly by *walker annihilation* [10]. This class of algorithms are all implemented in the HANDE-QMC package [11].

2. Reviews

2.1. Full configuration interaction

Full configuration interaction (FCI), also known as exact diagonalisation to physicists, is the exact eigendecomposition of a Hamiltonian in a given basis set. FCI yields the exact ground (and excited) state energies, and FCI calculations are sought after as the true benchmark for other electronic structure methods. A Hartree-Fock (HF) calculation with M basis functions and N electrons gives a set of $2M$ one-particle spin-orbitals ψ_i, and the approximate ground state, $|\Psi_{\mathrm{HF}}\rangle$, for the system is the one in which the electrons fill the eigenfunctions according to the *aufbau* principle, here given in an second-quantisation occupation-number (ON) vector [12, p. 1]:

$$|\Psi_{\mathrm{HF}}\rangle = |\underbrace{1,\ldots,1}_{N},\underbrace{0,\ldots,0}_{2M-N}\rangle \tag{4}$$

The basis for FCI is the set of all possible excitations from $|\Psi_{\mathrm{HF}}\rangle$:

$$|k_1,k_2,\ldots,k_{2M}\rangle,\ k_P = \begin{cases} 1 \text{ if } \psi_P \text{ occupied} \\ 0 \text{ if } \psi_P \text{ unoccupied} \end{cases}, \tag{5}$$

with the total number of occupied states fixed at N. For a close-shell system, there will be $\binom{M}{N/2}^2$ basis functions for FCI, hence its formal factorial ($\mathcal{O}(N!)$) scaling (not to be confused with the 'exponential wall' first introduced by Walter Kohn in his Nobel lecture [13], which is about the number of variational parameters, which scales like p^{3N}, with p being the number of variational parameters per spatial degree of freedom).

The most efficient FCI algorithms are based on the vectorised string formalism of Handy and Knowles [14], and improvements thereof [15], for a review, see [16].

The largest FCI calculations to date involve at most about 10^{10} Slater determinants, on relatively modest systems such as N_2 [17], AlP [18], pentacene and Cr_3 [19].

If the allowed excitations are limited in Equation (5), then a series of approximations to full CI can be obtained, known as CISD (CI with **s**ingles and **d**oubles excitations), CISDT (**t**riples), CISDQ (**q**uadruples), CISDTQ5, and so on. Their scaling is $\mathcal{O}(N^{2M+2})$, where M is the truncation level [16]. However, unlike other systematically truncated methods such as Møller-Plesset perturbation theory and coupled-cluster theory, truncations of FCI are not size-consistent (where the total correlation energy scales linearly with the size of the system), and as a whole less useful, especially in larger systems.

The HANDE-QMC package implements a rudimentary (F)CI solver, which simply generates the full Hamiltonian and uses one BLAS `?syev` call to diagonalise it. Due to the exponential scaling of the full Hamiltonian, the module needs to be massively parallelisable, as the generation of the full Hamiltonian is usually the most time-consuming step. This is achieved by ScaLAPACK [20], which is a BLAS/LAPACK implementation with MPI parallelisation, based on a *two-dimensional block cyclic* data distribution. As it needs additional arguments such as the MPI communicator (known as the 'context'), and identifiers for the position of the local array section in the globally distributed array, ScaLAPACK cannot keep the same familiar LAPACK inter-

faces intact and has to append the LAPACK routine names by 'p'.

2.2. Approximate FCI schemes

If only the few lowest (or highest) eigenpairs are needed, approximate diagonalisation schemes exist, and they generally belong to the *subspace iteration* class of methods, which include Lanczos algorithm [21] and the Davidson-Liu method [22], with the latter essentially a preconditioned version of the former. It has become the *de facto* standard approximation to FCI owing to its numerical stability [16].

As part of this report, the Davidson's method was implemented in the HANDE-QMC [11] software package, where it is interfaced with the rest of the code to perform approximate FCI calculations on the UEG and molecular systems. The outline of the Davidson-Liu algorithm is as follows [23, 24]. For a quantum mechanical Hamiltonian $\hat{\mathbf{H}}$ in a finite basis $\{|D_\mathbf{i}\rangle\}$ (where the subscript $\mathbf{i}$ denotes an ON vector) of size N, the Hamiltonian element is given by $H_\mathbf{ij} = \langle D_\mathbf{i}|\hat{\mathbf{H}}|D_\mathbf{j}\rangle$. For the lowest m eigenpairs sought, $k > m$ orthonormal trial vectors (where conventionally $k \approx 2m$) of length N are gathered in an array V. The *subspace Hamiltonian*, also known as the *Rayleigh matrix* is then constructed:

$$\mathbf{T} = (\mathbf{V})^T\mathbf{H}\mathbf{V} \tag{6}$$

and then diagonalised:

$$\mathbf{T}\mathbf{C} = \mathbf{C}\mathbf{t} \tag{7}$$

where $\mathbf{C}$ holds the CI coefficients for the best approximation to the k-lowest eigenvectors, and $\mathbf{t}$ is a diagonal matrix holding the corresponding eigenvalues. The approximate eigenvectors, also known as the *Ritz vectors*, are calculated:

$$r_\mu^{(i)} = V_{\mu\nu}C_{\nu i} \tag{8}$$

and then the *residual vectors*:

$$w_\nu^{(i)} = H_{\mu\nu}r_\mu^{(i)} \tag{9}$$

which should approach $\mathbf{0}$ as the iterations converge. These are then preconditioned with the *Jacobi preconditioner* to give the new trial vectors:

$$\boldsymbol{q}^{(i)} = \frac{\boldsymbol{w}^{(i)}}{t_\mathbf{ii} - H_\mathbf{ii}} \tag{10}$$

which is appended to the array $\mathbf{V}$. After all k new trial vectors are added in, an orthonormalisation procedure is carried out on $\mathbf{V}$, which is usually done with a QR decomposition, with common algorithms including the Gram-Schmidt process, the Householder transformation [25] (which is the algorithm used by the `BLAS` QR decomposition routines `?geqrf`), and Givens rotations. Then the subspace Hamiltonian is constructed again and the process repeats.

When $\mathbf{V}$ exceeds a pre-set size of d_max, a *subspace collapse* can be carried out, where only the k lowest approximate eigenvectors are retained, this is known as the *dynamic thick restarting* of the method [26]:

$$V_{\mu i} \leftarrow V_{\mu j}C_{ji},\ 1 \le i \le k,\ 1 \le j \le d_\text{max} \tag{11}$$

2.3. FCIQMC

Continuing from Equation (3), we can choose the initial trial wavefunction as the Hartree-Fock reference function, Ψ^HF. We can expand Ψ^HF formally in a basis of the FCI eigenvectors:

$$|\Psi^\text{HF}\rangle = \sum_i c_i|\Psi_i^\text{FCI}\rangle \tag{12}$$

where each of the FCI eigenvectors are themselves linear combinations of various excitations of Ψ^HF. The exponential projection operator has the following effect:

$$e^{-\tau(\hat{\mathbf{H}}-S)}|\Psi^\text{HF}\rangle = \sum_i e^{-\tau(\epsilon_i - S)}|\Psi_i^\text{FCI}\rangle \tag{13}$$

It can be seen that the effect is to exponentially decay away excited FCI states:

$$\lim_{\tau\to\infty} e^{-\tau(\hat{\mathbf{H}}-S)}|\Psi^\text{HF}\rangle = |\Psi_0^\text{FCI}\rangle,\ \text{for } S = \epsilon_0 \tag{14}$$

At this point, the equation is written in an iterative form

$$\Psi(\tau + \delta\tau) = e^{-\delta\tau(\hat{\mathbf{H}}-S)}\Psi(\tau) \tag{15}$$

and approximated by a first-order Taylor expansion

$$\Psi(\tau + \delta\tau) = [1 - \delta\tau(\hat{\mathbf{H}} - S)]\Psi(\tau) \tag{16}$$

Left-multiplying with $\langle D_\mathbf{i}|$ and integrating to reveal the CI coefficients, we have

$$\begin{aligned} C_\mathbf{i}(\tau + \delta\tau) &= C_\mathbf{i}(\tau) \\ &- \delta\tau(H_\mathbf{ii} - S)C_\mathbf{i}(\tau) - \delta\tau\sum_{\mathbf{j}\neq\mathbf{i}} H_\mathbf{ij}C_\mathbf{j}(\tau) \end{aligned} \tag{17}$$

The timestep, $\delta\tau$ obeys the relation, in common with DMC

$$\delta\tau \le \frac{2}{E_\text{max} - E_0} \tag{18}$$

with the denominator known as the *spectral radius* of $\hat{\mathbf{H}}$, and is easily seen as a result of the requirement that the following power iterations do not diverge:

$$\lim_{N\to\infty}[1-\delta\tau(\hat{\mathbf{H}}-S)]^N\Psi(0) \tag{19}$$

Equation (17) can be now transparently translated into a walker-based Monte Carlo algorithm, which is schematically depicted in Figure 1, where signed walkers reside on determinants $|D_{\mathbf{i}}\rangle$ whose signed walker population signifies their CI coefficients $C_{\mathbf{i}}$:

1. **Initialisation**: an initial distribution of walkers is generated, usually just on the Hartree-Fock reference $|D_{\mathbf{0}}\rangle$.
2. **Cloning and death**: the diagonal action of the Hamiltonian is sampled, where the walker 'dies' or is 'cloned', depending on the sign of the probability, on the same determinant with a probability proportional to $\delta\tau(H_{\mathbf{ii}}-S)C_{\mathbf{i}}(\tau)$.
3. **Spawning**: the off-diagonal action of the Hamiltonian is sampled, where for each walker, a walker can be created on a connected determinant (*i.e.*, $H_{\mathbf{ij}}\neq 0$ or that the bit-string (Hamming) distance of $\mathbf{i}$ and $\mathbf{j}$ is no more than two), with a probability proportional to $\delta\tau H_{\mathbf{ij}}$.
4. **Annihilation**: for every determinant that is populated, positive and negative walkers cancel each other out. This prevents the sign problem where the representations of Ψ and $-\Psi$ grow together, causing uncontrollable noise. This concludes a Monte Carlo step, return to step 2.

At the beginning of each run, the arbitrary shift is generally fixed at the HF reference energy, enabling exponential growth of total walker population, driven by the scarcity of death events. However, after a system-specific target population is reached, the shift is allowed to become negative to match E_{corr}. The target population is usually determined by running an unrelaxed calculation (*i.e.*, with a very large target population), and observing the height of the plateau in a plot of total population against iteration.

2.4. CCMC

The formulation of CCMC closely matches that of FCIQMC, with the difference that instead of residing on determinants, walkers reside on *excitors*, $\hat{a}_{\mathbf{n}}$, defined as $\hat{a}_{\mathbf{n}}|D_{\mathbf{0}}\rangle = |D_{\mathbf{n}}\rangle$. Replacing the FCI wavefunction by the coupled-cluster *ansatz* in Equation (16) and left-multiplying by $\langle D_{\mathbf{i}}|$ gives

$$\begin{aligned}\langle D_{\mathbf{i}}|\Psi^{\text{CC}}(\tau+\delta\tau)\rangle =&\langle D_{\mathbf{i}}|\Psi^{\text{CC}}(\tau)\rangle\\ &-\delta\tau\langle D_{\mathbf{i}}|(\hat{\mathbf{H}}-S)|\Psi^{\text{CC}}(\tau)\rangle\end{aligned} \tag{20}$$

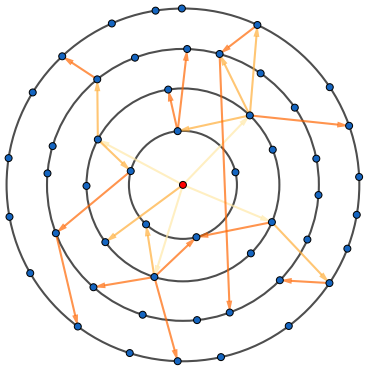

Figure 1: Schematic representation of the FCIQMC propagation. The central red dot is the reference determinant, and the arrows represent spawning, with darker colors representing more recent Monte Carlo moves. The innermost ring represent the space of single excitations, and the next doubles, and so on. Assuming a restricted HF reference, only double excitations will be spawned in the first iteration due to Brillouin's theorem.

We now have to consider an additional complication, that the coupled-cluster *ansatz* parametrises the wavefunction with cluster amplitudes in a non-linear fashion, as compared to the linear CI coefficient parametrisation in FCI:

$$\begin{aligned}&|\Psi^{\text{CC}}\rangle = e^{\hat{T}}|\Psi^{\text{HF}}\rangle\\ &\hat{T}=\sum_{\mu}^{\kappa}\hat{T}_{\mu},\ \kappa\text{ being the truncation level,}\\ &\hat{T}_{\mu}=\sum_{\substack{\text{unique}\\ \mu-\text{tuple}}} t^{a\ldots}_{i\ldots}\hat{\tau}^{a\ldots}_{i\ldots},\ \hat{\tau}^{a\ldots}_{i\ldots}=\hat{a}^{\dagger}_{a}\hat{a}_{i}\ldots,\end{aligned} \tag{21}$$

Of course, the CI coefficients can be extracted by a simple projection, but in general it will contain contributions from multiple clusters. For example of a CCSD wavefunction (*i.e.*, $\hat{T}=\hat{T}_1+\hat{T}_2$)

$$\langle D^{ab}_{ij}|e^{\hat{T}}|\Psi^{\text{HF}}\rangle = t^{ab}_{ij}+t^{a}_{i}t^{b}_{j}-t^{b}_{i}t^{a}_{j} \tag{22}$$

with the negative sign arising from the fact that $\hat{a}^{\dagger}_{b}\hat{a}_{i}\hat{a}^{\dagger}_{a}\hat{a}_{j}=-\hat{a}^{\dagger}_{a}\hat{a}_{i}\hat{a}^{\dagger}_{b}\hat{a}_{j}$, due to the anticommutation relations of the second-quantised creation and annihilation operators [12, p. 8]. Terms like t^{ab}_{ij} are known as *non-composite* cluster amplitudes, and the rest as *composite* cluster amplitudes. Here we make the approximation that composite clusters have much smaller contributions than the non-composite ones, their changes will be negligible per time step, and hence we can cancel out the $\mathcal{O}(\hat{T}^2)$ contributions on both sides to write

$$t_{\mathbf{i}}(\tau+\delta\tau)\rangle = t_{\mathbf{i}}(\tau)-\delta\tau\langle D_{\mathbf{i}}|(\hat{\mathbf{H}}-S)|\Psi^{\text{CC}}(\tau)\rangle \tag{23}$$

To accommodate this complication, an additional step needs to be performed for each Monte Carlo iteration, that is the sampling of the exponential *ansatz*: for N_{ex} total walkers, also called *excips* in CCMC, $\mathcal{O}(N_{\text{ex}})$ clusters are formed randomly by combining them according to specific biasing rules [27]. For each cluster, instead of looping over all connected determinants like in FCIQMC, only one spawning attempt is made per sampled cluster, as the looping cost would scale prohibitively as $\mathcal{O}(N_{\text{ex}}^2)$ instead of number of occupied determinants like in FCIQMC.

Another complication is related to *intermediate normalisation* in the coupled-cluster formalism [28, p. 20]:

$$\langle D_{\mathbf{0}}|\Psi^{\text{CC}}\rangle \equiv 1 \tag{24}$$

However this means that Equation (20) cannot update the case for $|D_{\mathbf{i}}\rangle = |D_{\mathbf{0}}\rangle$. This is solved by introducing a new independent variable N_0, the *reference population*, and re-writing the CC *ansatz* as $N_0 e^{\hat{T}/N_0}|D_{\mathbf{0}}\rangle$. This means that the reference population can be varied like populations on any other excitor.

2.5. Estimators

As stochastic algorithms, all physical observables in FCIQMC and CCMC are approximated by estimators, the simplest of which is the estimator for the expectation value of a variable O: $\langle O\rangle = \frac{1}{N}\sum_{i=1}^{N} O_i$.

However the variance of the variable is also needed to gauge the error in the estimates. Naively this can involve time auto-correlation functions, reviewed in [29, Sec. III], which is computationally expensive and requires some subjective choices.

A more economical method, known as the *blocking method*, was recapitulated in the same paper. The HANDE-QMC package uses the blocking method [30] to obtain error bounds on all observable quantities.

The main realisation behind the blocking method is that the expectation value and the variance are invariant under a *blocking transformation* where a new data set of half the size is obtained from taking sets of averages of adjacent data points in the original data set; and also that the lower bound of the variance approaches the true value every time a blocking transformation is applied.

2.5.1. The shift parameter

As alluded to above, the arbitrary shift parameter S is kept constant at the start of a simulation to grow the total population so that the correct sign structure of the ground state is represented, and then allowed to relax to serve as an estimator of the ground state energy. The update is performed every A steps, and is given by [7]:

$$S(\tau + A\delta\tau) = S(\tau) - \frac{\zeta}{A\delta\tau}\ln\frac{N_w(\tau + A\delta\tau)}{N_w(\tau)} \tag{25}$$

where N_w is the number of walkers as a function of imaginary time, and ζ is a dampening factor. The shift is guaranteed to converge onto the true ground state energy as Equation (25) reduces the shift if there's a net gain in walkers in a set of A steps, signifying that the shift is higher than the ground state energy (alternatively $\mathbf{H} - S\mathbf{I}$ has at least one positive eigenvalue); and conversely the shift is raised if it is lower than the ground state energy, and when the population is stationary, signifying that the zero eigenvector, *i.e.*, the ground state vector of $\mathbf{H} - S\mathbf{I}$ has been located.

2.5.2. The projected energy

Another, independent estimator for energy is the *projected energy*:

$$\begin{aligned} E_{\text{proj}}(\tau) &= \frac{\langle D_{\mathbf{0}}|\hat{\mathbf{H}}|\Psi(\tau)\rangle}{\langle D_{\mathbf{0}}|\Psi(\tau)\rangle} \\ &= \langle D_{\mathbf{0}}|\hat{\mathbf{H}}|D_{\mathbf{0}}\rangle\frac{N_{\mathbf{0}}(\tau)}{N_{\mathbf{0}}(\tau)} + \sum_{\mathbf{j}\neq\mathbf{0}}\langle D_{\mathbf{j}}|\hat{\mathbf{H}}|D_{\mathbf{0}}\rangle\frac{N_{\mathbf{j}}(\tau)}{N_{\mathbf{0}}(\tau)} \\ &= E^{\text{HF}} + \sum_{\mathbf{j}\neq\mathbf{0}}\langle D_{\mathbf{j}}|\hat{\mathbf{H}}|D_{\mathbf{0}}\rangle\frac{N_{\mathbf{j}}(\tau)}{N_{\mathbf{0}}(\tau)} \end{aligned} \tag{26}$$

In FCIQMC, after each iteration, this sum is explicitly performed over singly and doubly excited determinants with respect to the HF determinant; in CCMC, as the parametrisation is non-linear, the numerator in Equation (26) would contain products of single cluster amplitudes, rendering direct looping infeasible.

2.6. Recent developments

FCIQMC and CCMC are both still under active development, under the HANDE-QMC package [11] (which also includes DMQMC) and the NECI package [31] (which only has FCIQMC).

2.6.1. The initiator approximation

Proposed for FCIQMC in [32] and adapted for CCMC [27], the initiator approximation reduces the total number of walkers needed to reach convergence. It does this by only allowing the spawns from a select few *initiator determinants* to survive. The initial set of initiator determinants is usually selected by a complete active space

(CAS) criterion, and may be dynamically modified according to a population criterion.

However the approximation does introduce a systematic error in the converged energy that becomes zero in the limit of very large walker populations. Various proposals were introduced to remove the *initiator error*, including using extrapolation [27, Sec. VI and Appendix A], or with a second-order Epstein-Nesbet (EN2) perturbation theory correction based on discarded spawning attempts [33].

2.6.2. The quasi-Newton acceleration

Proposed in [34], in which Equation (16) is viewed as a steepest-descent update equation, and naturally replaceable by any other optimisation algorithm:

$$\boldsymbol{c}(\tau + \delta\tau) = \boldsymbol{c}(\tau) - \delta\tau \mathbf{A}\boldsymbol{g}(\tau) \tag{27}$$

where $\boldsymbol{g} = (\mathbf{H} - \mathbf{I}S)\boldsymbol{c}$ is the gradient, and $\mathbf{A} = \widetilde{\mathbf{H}}^{-1}$ is the Hessian:

$$\widetilde{H}_{\mathbf{ij}} = \frac{\partial g_{\mathbf{i}}}{\partial c_{\mathbf{j}}} \propto \langle D_{\mathbf{i}}|\hat{\mathbf{H}} - S|D_{\mathbf{j}}\rangle \tag{28}$$

The inversion of the exact Hessian is manifestly exponentially expensive. However, as the FCI Hamiltonian is diagonally dominant, $\widetilde{\mathbf{H}}$ can be approximated by zeroing all the off-diagonal elements. This essentially has the effect of weighting the Hamiltonian elements by appropriate sums of HF orbital energies in spawning:

$$p_{\text{spawn}}(\mathbf{i} \to \mathbf{j}) \propto \delta\tau \frac{\langle D_{\mathbf{i}}|\hat{\mathbf{H}}|D_{\mathbf{j}}\rangle}{E(D_{\mathbf{j}})} \tag{29}$$

where $E(D_{\mathbf{j}})$ is the difference in energy between $D_{\mathbf{i}}$ and $D_{\mathbf{0}}$:

$$E(D_{\mathbf{j}}) = \sum_{i \text{ in } \mathbf{j}} \epsilon_i - \sum_{i' \text{ in } \mathbf{0}} \epsilon_{i'} \tag{30}$$

However, the death step (diagonal action of the Hamiltonian), originally written as

$$p_{\text{death}}(\mathbf{i}) \propto \delta\tau \langle D_{\mathbf{i}}|\hat{\mathbf{H}} - S|D_{\mathbf{i}}\rangle \tag{31}$$

cannot simply be scaled due to the determinant-dependence of the scaling factor, which can cause the true solution to drift if S is not equal the correct energy (S, in this sense, is a less true estimator of the energy as the imaginary time evolution is discretised). To address this, the death step is modified with the introduction of a new population control variable ρ:

$$p_{\text{death}} \propto \delta\tau \left[\frac{\langle D_{\mathbf{i}}|\hat{\mathbf{H}} - E_{\text{proj}}|D_{\mathbf{i}}\rangle}{E(D_{\mathbf{i}})} + \rho(E_{\text{proj}} - S) \right] \tag{32}$$

where the projected energy E_{proj} will always be the true energy at if we have the true solution, and hence will not cause a similar drift if the shift is used.

The quasi-Newton algorithm in HANDE provides for a few input parameters, the '`quasi_newton_threshold`', Δ_{QN}, is a cut-off value for the small $E(D_{\mathbf{j}})$, and serves as a numeric device to avoid division by small numbers, and the '`quasi_newton_pop_control`', ρ, is the same variable in Equation (32), and is usually set to the same value as Δ_{QN}.

2.6.3. Jacobi preconditioning

Suggested in [35], in common with the quasi-Newton approach, the starting point is viewing the imaginary time propagation from a different angle, this time as an iterative eigenvalue problem, of which the Davidson's method introduced in Section 2.2 is one. The general form of an iterative step is

$$\boldsymbol{c}^{(n+1)} = \boldsymbol{c}^{(n)} - \gamma^{(n)}\mathbf{P}^{-1}[(\mathbf{H} - \mathbf{I}S^{(n)})\boldsymbol{c}^{(n)}] \tag{33}$$

where $\mathbf{P}$ is the *preconditioner*, which is the identity matrix in the original FCIQMC and CCMC algorithms. Note the equivalence of this equation with Equation (27) when $\gamma^{(n)} = \delta\tau$. The Jacobi preconditioner, exactly the same one used in Equation (10), is given by

$$P_{\mathbf{ij}} = (H_{\mathbf{ii}} - S)\delta_{\mathbf{ij}} \tag{34}$$

This then can be straightforwardly translated to simple modifications in the spawning (off-diagonal) and death (diagonal) routines. In spawning, each spawned walker will have its amplitude multiplied by $1/(H_{\mathbf{ii}} - S)$, and in death, every determinant will have its amplitude multiplied by $1 - \delta\tau$. A further modification to ensure controllable stochastic noise is to allow each walker to have multiple spawning attempts N_{spawn}, with the resulting spawns' amplitudes divided by N_{spawn}.

The Jacobi preconditioner has allowed much larger (up to unity is reported) time steps, however, the need to use a rather large N_{spawn}, essentially dividing $\delta\tau$ by N_{spawn}, cancels most of the time savings (see for example figure 6 in [35]).

2.6.4. Excitation generators

The spawning step occurs $\mathcal{O}(N_{\text{ex}})$ times in each Monte Carlo step, which represents the bulk of the computational cost of FCIQMC and CCMC, therefore it is essential to perform each step as efficiently as possible. The excitation generator, in its essence, generates a connected $|D_{\mathbf{n}}\rangle$ given a determinant $|D_{\mathbf{m}}\rangle$, given information about the associated probabilities $p_{\text{gen}} = p(\mathbf{n}|\mathbf{m})$.

A 'renormalised' uniform excitation generator is used in the original FCIQMC and CCMC (see [7] and fig. 5 of [36]), but recently it has been noted that since the spawn probability is

$$p_{\text{spawn}} \propto \frac{\delta\tau}{p_{\text{gen}}}|H_{\mathbf{nm}}| \tag{35}$$

for an efficient algorithm, p_{spawn} should be roughly constant to ensure both stable dynamics and sustained sampling of important regions of the phase space. This means p_{gen} should be proportional to $|H_{\mathbf{nm}}|$.

The heat-bath excitation generator, first proposed by [37], does exactly this, by pre-computing all Hamiltonian elements, at a memory cost of $\mathcal{O}(M^4)$. A less memory-intensive version is suggested by [38], together with combinations with other numerical approximations such as the Cauchy-Schwarz and Power-Pitzer inequalities [39]:

$$|\langle ij|ab\rangle|^2 \leq \langle ia|ia\rangle\langle jb|jb\rangle \text{ (Cauchy-Schwarz)} \tag{36a}$$

$$|\langle ij|ab\rangle|^2 \leq \langle ia|ai\rangle\langle jb|bj\rangle \text{ (Power-Pitzer)} \tag{36b}$$

Another algorithm, known just as the *Cauchy-Schwartz* excitation generator [31, Appendix 2] also approximates p_{gen} to keep p_{spawn} roughly constant.

2.6.5. Even selection and full non-composite

These two modification are relevant for CCMC only. A consequence of the original CCMC algorithm is that both the spawning and death probabilities of a cluster are proportional to

$$\frac{w_e}{n_a p_{\text{select}}(e)} = \frac{2^{s+1}}{s!}\left(\frac{N_{\text{ex}}}{N_0}\right)^{s-1} \tag{37}$$

where $p_{\text{select}}(e)$ is the probability of selecting a combination of excitors e with the product of weights on them being w_e, and s is the number of excitors involved in forming the cluster. Given that $N_{\text{ex}}/N_0 > 1$ normally, this means that large, composite clusters have much larger spawning and death probabilities compared to non-composite ones. This causes what is known as 'blooms', in which a large amount of walkers being generated on a relatively unimportant excitor, potentially causing the overlap between the stochastic wavefunction and the true wavefunction to be too small for continued projection (analogous to being ejected from the 'valley' of the correct solution), and also creating load balancing and memory requirement issues.

The solutions proposed in [40] aim to address blooms by fixing $w_e/p_{\text{select}}(e)$ to be unity. The first and partial solution is termed *full non-composite*, which fixes the above-mentioned quantity to unity only for the non-composite clusters, *i.e.*, for $s = 0, 1$, by explicit looping of all reference, single and double excitors. This approach already shows significant improvements in calculation stability and especially reduced noise in the projected energy, as it only involves single and double excitors, which are all exactly sampled.

The second solution essentially removes the possibility of blooms, by requiring that the quantity be fixed at unity for all s, arriving at

$$n_a = N_{\text{ex}} \sum_{s=0}^{l+2} \frac{1}{s!}\left(\frac{N_{\text{ex}}}{N_0}\right)^{s-1} \tag{38}$$

which shows that the number of attempts scales exponentially with higher truncation levels. It then suggests ways that this exponential increase may be alleviated, by *truncated selection*. However in practice even selection does increase the computational cost appreciably. A cheap replacement is using full non-composite with the `cluster_multispawn_threshold` keyword, which splits up blooms into multiple spawning attempts.

2.7. Uniform electron gas

The uniform electron gas (UEG), also known as jellium, homogeneous electron gas (HEG), or uniform electron liquid (UEL), is a quantum mechanical model system favoured for its minimalistic and tunable description of electron correlation It is controlled by a single parameter, the Wigner-Seitz radius, which is the radius of a sphere containing one electron, given by

$$r_s = \sqrt[3]{\frac{3}{4\pi n}} \tag{39}$$

where n is the number density of electrons. The model describes a uniform electron distribution in a background of positive charge density such that the system is neutral. In the high-density (low r_s) regime, kinetic energy dominates and the non-interacting, free electron gas (FEG) is recovered [41, Ch. 1.3.3], whose exact ground state is trivial. As the density decreases the UEG goes through a series of non-trivial phases such as the spin-polarised ferromagnetic Fermi fluid at intermediate densities, and the exotic Wigner crystal at very low densities. The Hamiltonian describing the system can be written as [41, eq. 1.1]:

$$\hat{\mathbf{H}} = -\frac{1}{2}\sum_i \nabla_i^2 + \frac{1}{2}\sum_{i\neq j}\frac{1}{r_{ij}} + \hat{\mathbf{H}}_{\text{e-b}} + \hat{\mathbf{H}}_{\text{b-b}} \tag{40}$$

where $\hat{\mathbf{H}}_{\text{e-b}}$ is the electron-background interaction energy, and $\hat{\mathbf{H}}_{\text{b-b}}$ is the constant background-background

electrostatic energy:

$$\hat{\mathbf{H}}_{\text{e-b}} = \iint \frac{\rho(\mathbf{r})n(\mathbf{R})}{|\mathbf{r}-\mathbf{R}|}\mathrm{d}\mathbf{r}\mathrm{d}\mathbf{R} \tag{41a}$$

$$\hat{\mathbf{H}}_{\text{b-b}} = \frac{1}{2}\iint \frac{n(\mathbf{R})n(\mathbf{R}')}{|\mathbf{R}-\mathbf{R}'|}\mathrm{d}\mathbf{R}\mathrm{d}\mathbf{R}' \tag{41b}$$

with ρ being the electron density and n being the positive charge density. The Hartree-Fock eigenvalues of the UEG are analytically known (see [42, p. 105], and alternative derivations [41, 43, 44, 45]):

$$\epsilon_k = \frac{1}{2}k^2 - \frac{k_\text{F}}{\pi}f(k/k_\text{F}) + \frac{1}{2}V_\text{Mad} \tag{42a}$$

$$f(x) = 1 + \frac{1-x^2}{2x}\ln\left|\frac{1+x}{1-x}\right| \tag{42b}$$

where $V_\text{Mad} \approx -2.837297(3/4\pi r_s^3 N_e)^{1/3}$, where N_e is the number of electrons per unit cell, is the Madelung constant introduced by finite size effects of using periodic boundary cells [46, 47]. The electron repulsion integrals are also analytically known [48]:

$$\langle ij|ab\rangle = \frac{4\pi}{\Omega|\boldsymbol{k}_i - \boldsymbol{k}_a|^2} \tag{43}$$

where Ω is the (real-space) volumn of the simulation cell. With these quantities able to be generated, FCIQMC and CCMC calculations can be run for arbitrary r_s and N_e.

The study of the UEG with QMC methods is a long-running one, with the seminal work by Ceperley and Alder [49], followed by refinements [50, 51], which used DMC to produce benchmark-quality phase diagrams for the UEG from high to very low density regimes. These results were then fitted to produce the *local density approximation* (LDA) correlation functionals, with commonly used ones including one due to Vosko, Wilk and Nusair (VWN, [52]), and one due to Perdew and Wang (PW91, [53]).

The study of UEG with coupled-cluster methods has been limited, and mostly in the thermodynamic limit (infinite cell size) [54, 55], with a few works in finite cells [27, 56, 48, 57]. Specifically, more study is needed in CCMC to understand the effect on convergence of some of the new algorithmic additions outlined in Section 2.6.

3. Davidson's method

3.1. Computational implementation

The HANDE-QMC package employs a Lua interface for input file parsing and more complicated use cases that can involve looping and getting input parameters from functions defined in the input Lua script. The code is also highly modularised, with well documented read-in interfaces with Lua and clearly named derived types that hold input parameters. This makes implementing and integrating new modules relatively easy, as all new parameters can be read in as a independent, new Lua table, into relevant derived types, which can be used in the new code.

Specifically, the Lua interface is contained in the `src/lua_hande_calc.f90` source file, in the `read_fci_in` subroutine, and code for the module proper is in the `src/fci_davidson.F90` file.

3.1.1. Linear algebra routines

As detailed in Section 2.2, four basic linear algebra routines, shown in Table 1, together with their corresponding BLAS routines, form the backbone of the algorithm.

Table 1: The linear algebra routines needed in the Davidson's algorithm, and their BLAS Fortran subroutine names.

Operation	BLAS routine
Matrix-matrix multiplication	`?gemm`
Matrix-vector multiplication	`?gemv`
Hermitian matrix diagonalisation	`?syev`
Orthogonalisation	`?geqrf`, `?orgqr`

The HANDE-QMC package compilation script takes care of the searching for an optimised BLAS implementation, such as Intel MKL or OpenBLAS [58]. These libraries are generally all multi-threaded, either with their own threading layer or with OpenMP.

To facilitate the calling of these routines, generic Fortran interfaces are set up in `lib/local/linalg.F90`, which is the Fortran way of overloading procedures. Furthermore, some BLAS routines like `?syev` require two passes, with the first one determining the optimal workspace size, which is automated in the interface. The QR-decomposition routine in BLAS is implemented in two parts: `?geqrf` performs the Householder transformation, returning the scalar factors of the elementary reflectors and the reflector vectors separately; `?orgqr` is the helper routine that returns the actual orthonormal matrix $\mathbf{Q}$. These two routines are wrapped together for ease of use.

3.1.2. Parameters

The input parameters are mostly self-explanatory and checks are performed against illegal input values (such as requesting more eigenvalues than trial vectors).

`ndavidson_eigv` sets the number of lowest eigenvalues requested, m; `ndavidson_trialvec` sets the number of trial vectors, k; `davidson_maxsize` sets the largest number of trial vectors allowed to be held in $\mathbf{V}$ before a subspace collapse is performed, $d_{\max}$; `davidson_tol` is the convergence tolerance of the norm of the residual vectors, with the recommended value of 10^{-6} to 10^{-3} [24]; and finally `davidson_maxiter` is the maximum number of iterations. If convergence is not reached the user will be asked to re-submit the calculation with different parameters.

3.1.3. Numerics

Referring to Equation (10), in cases where the lowest $k \times k$ block of the Hamiltonian is already block-diagonal, or very nearly so, some of the $t_{\mathbf{ii}} - H_{\mathbf{ii}}$ will be exactly zero or very small, which will lead to either floating point errors or a very large guess vector being generated. To remedy this, the preconditioning step was modified with a level shift in the denominator:

$$\boldsymbol{q}^{(i)} = \frac{\boldsymbol{w}^{(i)}}{t_{\mathbf{ii}} - H_{\mathbf{ii}} + \Delta} \tag{44}$$

where $\Delta = 10^{-3}$ if $|t_{\mathbf{ii}} - H_{\mathbf{ii}}| < 10^{-3}$, essentially limiting the largest preconditioner to be approximately 10^3. Although not rigorously justified in theory, in practice the introduction of the level shift has not resulted in any systematic error in the results.

3.1.4. Results

Three systems, one being the UEG, and two molecular systems (where truncated CI calculations were performed) were tested, see Table 2. It was found that Davidson's method is capable of approaching exact FCI energies with essentially arbitrary precision, controlled by the residual tolerance parameter, while requiring a fraction of the computational resource. However, the agreement with FCI degrades gradually in excited states. But they are still mostly within chemical accuracy (± 1 kcal/mol), if only the lowest few excitations, which are the most chemically relevant ones, are sought.

4. Converging CBS UEG results

As part of the investigation into the performance of CCMC on UEG systems, benchmark-level, complete basis set (CBS) limit energies were produced.

Extrapolation methods are commonly used in producing CBS results in quantum chemistry [59, Ch. 5.9-5.13]. Many commonly used Gaussian basis sets can be enlarged systematically, for example, the Dunning basis sets ((aug)-cc-p(C)VnZ) [60], the Pople basis sets (X-YZ(++)G(**)) [61], and the Karlsruhe/Ahlrichs basis sets (def2-nVP(PP)(D)) [62, 63]. Using this fact, procedures have been devised that are themselves systematically improvable [59, Ch. 5.10], and largely based on empirical curve-fitting. They are known to produce excellent agreement with experiments [64, 65, 66].

For plane-wave basis sets as employed in the UEG systems, convergence is more straightforward, and usually a power-law relationship holds between the cutoff energy k_c or the number of plane waves, M, included in the basis set: see Figure 2 a schematic view of the reciprocal lattice of the UEG for the same r_s but different N_e, with k_F indicating the extent of the Fermi surface, within which reside occupied orbitals, and in the annular region are virtual orbitals. For a CBS study on the UEG with MP2 theory, [48] found a simple linear dependence of E_{corr} at very small $1/M$, whereas [57] extended this to up to cubic for bigger $1/M$.

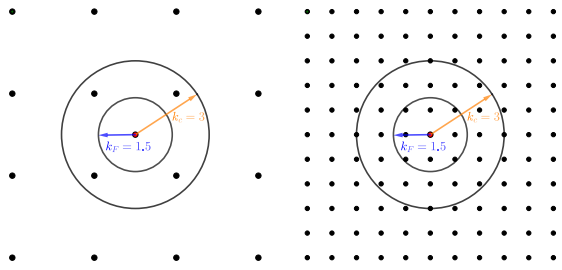

Figure 2: Schematic representation of the relationship between the energy cutoff k_c, and the number of plane wave basis functions M, represented by the number of points within the larger circle. Of course, the reciprocal lattice would be three-dimensional in a 3D UEG, and the circles will be spheres. The figure on the left would represent $N = 2$, as only one basis function is occupied, and $M = 5$, whereas the one on the right represents $N = 18$ and $M = 29$.

4.1. Methods

As the extrapolating functional form is not fixed by theoretical arguments (see [67] and references within), the more flexible scheme of [57] is adopted.

Figure 3 shows an example of such extrapolation result: 14 production runs with different M were performed and their results were obtained from a reblocking analysis. The full set of data is fitted with the `scipy.optimize.curve_fit` function [68], with up to cubic dependence on $1/M$, producing the 'full' curves, and an optimisation of $\chi^2/(N-1)$, where N is the number of data points, over the removal of the largest $1/M$ values, is performed, yielding the 'opt' curves. The χ^2

Table 2: Comparisons between Davidson's method and exact diagonalisation, timings were obtained with one hardware thread, on an i7-5820K @ 3.30GHz CPU.

System	LAPACK		Davidson	
	E / E_h	Time / s	E / E_h	Time / s
$4e$ 3D UEG, $r_s = 2\ a_0$	1.285524498812 1.285524498812 1.323763083919 1.323763083919	11.85	1.285524498905 1.285529430731 1.323763552821 1.323769231357	0.12
H_2 / cc-pVTZ CISD	−1.145758846665 −0.622330308365 −0.538417004463 −0.365633764501	0.10	−1.145758846665 −0.622330308365 −0.538417004463 −0.365633764501	0.08
Ne / cc-pVDZ CISDT	−128.676399416807 −127.037283769805 −126.907544390006 −126.907544390006	29.34	−128.676399416725 −127.037196880562 −126.905587739908 −126.871845067351	6.94

metric is used instead of the more simplistic root-mean-square deviation to take into account of the intrinsic uncertainties in each of the data points (obtained from reblocking), with the metric given as

$$\chi^2 = \sum_i \frac{[E_i - f(1/M)]^2}{\sigma(E_i)} \tag{45}$$

where $f(1/M)$ is a fitted function, and $\sigma(E_i)$ is the standard deviation of the i-th E_{corr} in the dataset.

The optimisation over removal of points is a rudimentary one: the values of $\chi^2/(N-1)$ over all $m \leq N \leq$ len(data), where m is the number of variational parameters, are stored in a vector, and a search is performed over it to determine the first local minimum, excluding the first and last points. This minimum is taken to represent the best compromise between uncertainty in the CBS result and the accuracy of fitting.

This is repeated for the linear, quadratic and cubic functional forms, where the y-intercept (E_{corr} at $1/M = 0$ limit) taken to be the CBS result, and the `scipy` function also reports the errors in these estimates. We accept the lowest polynomial model whose y-intercept agrees within 2σ of a higher-order polynomial model. The fitting procedure returns the following optimised CBS results for the 14-electron $r_s = 1.0$ CCSD UEG, on the linear, quadratic and cubic models respectively: $-0.5145(9)$, $-0.513(10)$, $-0.513(11)$. Although the quadratic and cubic results agree more closely, the simpler linear model was accepted as it agreed with the quadratic result within 2σ.

4.2. Results

As described in Section 2.4, the shoulder height for each system has to be determined before production calculations can be carried out. Figure 5 shows an example of a shoulder plot which is a plot of N_{ex}/N_0 against N_{ex}. In this case, the exact shoulder height is slightly ambiguous: the highest point on the curve is $\approx 3 \times 10^5$, but the hump could have been created by stochastic noise. In the interest of lower computational cost, the lower shoulder height of 6×10^4 was tested and gave stable calculations, showing that calculation stability is quite insensitive of the shoulder height. Also, the timestep, $\delta\tau$ also has to be estimated at this stage, where the largest timestep that does not cause significant blooms is chosen. Although HANDE provides for the automatic estimation of $\delta\tau$, in our limited testing bloom events still occurred too frequently, and sometimes resulted in early termination of

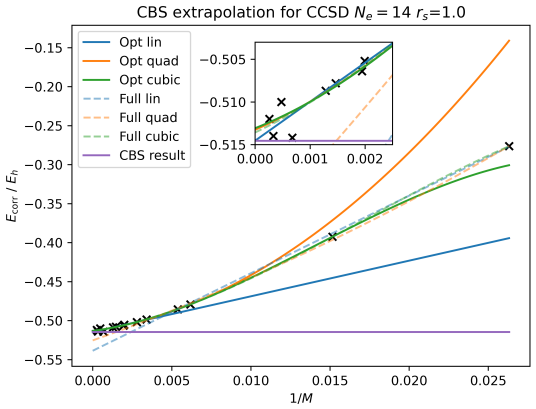

Figure 3: Extrapolated complete basis set limit results for CCSD $N = 14$, $r_s = 1.0$. The linear fit was taken to be the definitive one.

the program.

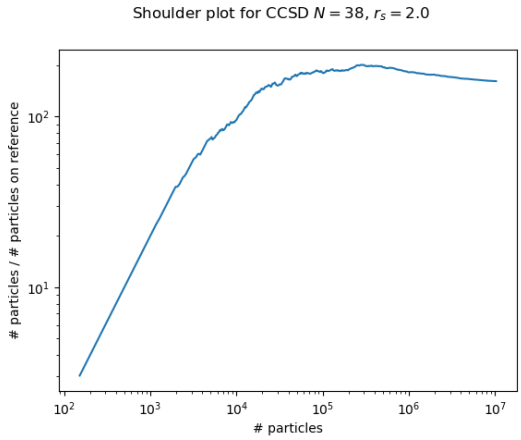

Figure 4: An example of a shoulder plot for a CCSD $N = 38$, $r_s = 2.0$ calculation. The shoulder height was estimated by eye to be 6×10^4.

The actual shoulder heights used in production calculations are presented in Figure 5, and the extrapolated CBS limit results for all the calculations attempted are presented in Table 3. Here we can see that for $N = 14$, CCSD is only sufficient for $r_s = 0.5$, whilst CCSDT is sufficient up to $r_s = 1.0$, mirroring the conclusion drawn in [57]; additionally we can also see that, for $N = 38$, CCSD is sufficient up to $r_s = 1.0$, suggesting that lower-order CC methods perform better for larger electron counts.

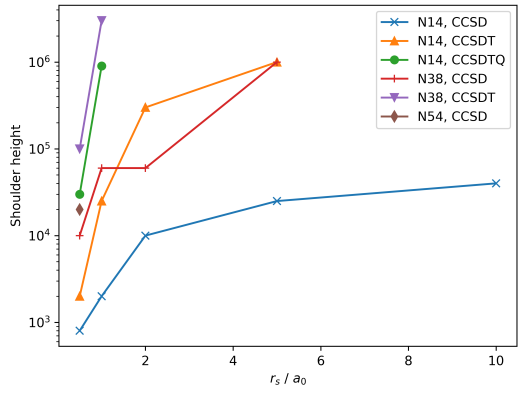

Figure 5: The shoulder heights determined for the systems under study. All shoulder heights higher than 10^6 were not pursued as production calculations would have been impractical within time constraints.

Table 3: CBS limit results for UEG systems of up to 54 electrons, up to CCSDTQ level, with FCIQMC benchmark results presented when available.

r_s / a_0	N	Truncation	CBS energy / E_h
0.5	14	CCSD	$-0.5865(6)$[1]
		CCSDT	$-0.5929(5)$
		CCSDTQ	$-0.5952(6)$
		FCIQMC	$-0.5969(3)$
	38	CCSD	$-1.825(7)$
		CCSDT	$-1.86(1)$[4]
		FCIQMC	$-1.849(1)$[2]
	54	CCSD	$-2.47(2)$
		FCIQMC	$-2.435(7)$[2]
1.0	14	CCSD	$-0.5146(9)$
		CCSDT	$-0.5334(4)$
		FCIQMC	$-0.5325(4)$[2]
	38	CCSD	$-1.59(11)$[3,4]
		FCIQMC	$-1.59(1)$ [2]
2.0	14	CCSD	$-0.4096(4)$
		CCSDT	$-0.4095(1)$
		FCIQMC	$-0.4447(4)$[2]
5.0	14	CCSD	$-0.2529(2)$
		FCIQMC	$-0.306(1)$[2]
	38	CCSD	$-0.763(7)$
10.0	14	CCSD	$-0.1566(3)$[3,4]

[1] The two lowest M points had to be removed.
[2] FCIQMC data taken from [69].
[3] No minima found, the full data set is used.
[4] The lowest M point had to be removed.

5. Parameter dependence of CCMC convergence

The CCMC module has recently been furnished with various algorithmic improvements, usually to improve speed of convergence or improve stability, oftentimes at a trade-off between the two. We aim to investigate the effects of these additions on the convergence of a small UEG system, the 14-electron, $r_s = 1.0$ system at CCSD. Hopefully this can serve as a prototype for bigger systems where exhaustive parameter-tuning studies are prohibitively expensive.

5.1. Method

This study is based on [34] which analysed the effects of the quasi-Newton approached on FCIQMC UEG and molecular systems. We are only interested in the projected energy at the beginning of the calculation, before the shoulder height is reached (here termed the 'hill-climbing phase'), as such every calculation is kept short by limiting the size of the state and/or spawning array, and in cases of large noise, just the iteration number. Each calculation is run with different random number

generator (RNG) seeds 20 times. [34] argued that the cost of each cycle scales as $\mathcal{O}(N_{\text{ex}})$, the computational cost, η, should be measured by the cumulative population, *i.e.*, $\eta = A\sum_i^M N_{\text{ex}}(\tau_i)$ where A is the number of cycles between reports, and M the total number of reports. However we also investigate the effect of even selection, which works by increasing $N_{\text{attempt}} = n_a$ (see Section 2.6.5), its true computational cost would be hidden if the cumulative population is used. For this reason we use $\eta = A\sum_i^M N_{\text{attempt}}(\tau_i)$. A is always set to 1 here for the ease of analysis. As η is a continuous variable, we need to bin it to obtain the average E_{proj} at a certain (binned) η, and its variance. These tasks are performed with the PyHANDE [30] and pandas [70] packages.

5.2. Results

The results are presented in Figure 6. It is immediately clear that the quasi-Newton algorithm, with the larger timesteps it allows, has a large effect on the convergence of calculation. We can also see that various other parameters can affect the stochastic noise in a calculation, but has no effect on convergence time, with the exceptions of quasi-Newton and even selection. The default excitation generator for UEG is '`norenorm`', which randomly generates excitations and rejects them if spin or spatial symmetry (in this case, crystal momentum conservation) is broken. The '`power-pitzer`' excitation generator (see Section 2.6.4) pre-calculates weights of choosing one of the excited orbitals in an effort to keep p_{spawn} approximately constant. This does not add to the computational cost significantly and should bring about reduced noise, as can be seen in the figure where the error bars of 'QN 0.001' is completely covered by that of 'QN 0.001 norenorm'. The effect of turning off even selection is also clear from the figure, as it approaches the CBS energy at a cost comparable to calculations with with much larger timesteps, however with somewhat larger noises. For completeness, we included the calculations where we set $\Delta_{\text{QN}} = 1$ (see Section 2.6.2). As expected, this does not affect any aspect of the calculation, as the HOMO-LUMO gap in this UEG system is a large finite number ($1.3077\ E_h$), and customising Δ_{QN} should only be done in strongly quasidegenerate or metallic systems.

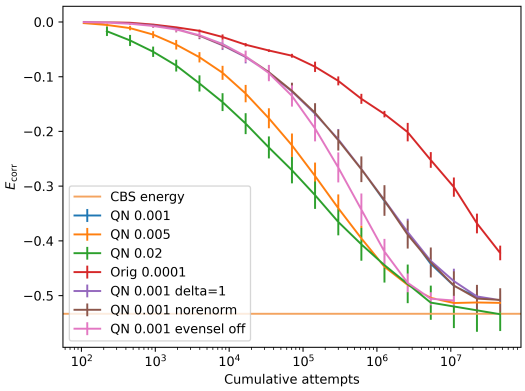

Figure 6: The effect of various parameters on the convergence of CCMC algorithm.

6. Future work

In the preparation of this report, the importance of the timestep as a central variable in controlling the computational cost is highlighted. Therefore, more work needs to be done in testing and refining the automatic $\delta\tau$ finding algorithm. In the other direction, algorithms that are less sensitive to the timestep need to be investigated - the wall-Chebyshev projector introduced in [71], which is completely independent of the timestep, is a promising candidate that will be investigated in an upcoming report.

7. Conclusions

We introduced the theoretical foundations of the coupled-cluster Monte Carlo algorithm in the context of approximations to the full configuration interaction, and briefly reviewed many of the recent algorithmic additions to it. We also introduced the uniform electron gas (UEG) as a model system of tunable electron correlation, and we obtained benchmark-level complete basis set limit results for 3D UEG systems containing up to 54 electrons with r_s up to $10.0\ a_0$, at truncations up to CCSDTQ. We also briefly studied the parameter dependence of CCMC convergence, and showed that the timestep is the most important parameter in controlling the computational cost of a calculation.

Acknowledgments

I would like to thank Maria-Andreea Filip and Nicholas Lee for their help in reviewing this report, the rest of the Thom group for their unwavering support, and my supervisor, Dr Alex Thom, for his kind words in times of stress and helpful discussions. This work used the ARCHER2 UK National Supercomputing Service (`https://www.archer2.ac.uk`).

References

[1] E. Y. Loh, J. E. Gubernatis, R. T. Scalettar, S. R. White, D. J. Scalapino, R. L. Sugar, Sign problem in the numerical simulation of many-electron systems, Physical Review B 41 (13) (1990) 9301–9307, publisher: American Physical Society. doi:10.1103/PhysRevB.41.9301.
URL https://link.aps.org/doi/10.1103/PhysRevB.41.9301

[2] E. Pavarini, E. Koch, U. Schollwöck (Eds.), Emergent Phenomena in Correlated Matter, Vol. 3 of Schriften des Forschungszentrums Jülich. Reihe modeling and simulation, Forschungszentrum Jülich GmbH Zentralbibliothek, Verlag, Jülich, 2013.
URL https://juser.fz-juelich.de/record/137827

[3] R. J. Needs, M. D. Towler, N. D. Drummond, P. L. Ríos, Continuum variational and diffusion quantum Monte Carlo calculations, Journal of Physics: Condensed Matter 22 (2) (2009) 023201, publisher: IOP Publishing. doi:10.1088/0953-8984/22/2/023201.
URL https://doi.org/10.1088/0953-8984/22/2/023201

[4] J. B. Anderson, A random-walk simulation of the Schrödinger equation: H+3, The Journal of Chemical Physics 63 (4) (1975) 1499–1503, publisher: American Institute of Physics. doi:10.1063/1.431514.
URL http://aip.scitation.org/doi/abs/10.1063/1.431514

[5] J. B. Anderson, Quantum chemistry by random walk. H 2P, H+3 D3h 1A'1, H2 3Σ+u, H4 1Σ+g, Be 1S, The Journal of Chemical Physics 65 (10) (1976) 4121–4127, publisher: American Institute of Physics. doi:10.1063/1.432868.
URL http://aip.scitation.org/doi/abs/10.1063/1.432868

[6] S. Zhang, H. Krakauer, Quantum Monte Carlo Method using Phase-Free Random Walks with Slater Determinants, Physical Review Letters 90 (13) (2003) 136401, publisher: American Physical Society. doi:10.1103/PhysRevLett.90.136401.
URL https://link.aps.org/doi/10.1103/PhysRevLett.90.136401

[7] G. H. Booth, A. J. W. Thom, A. Alavi, Fermion Monte Carlo without fixed nodes: A game of life, death, and annihilation in Slater determinant space, The Journal of Chemical Physics 131 (5) (2009) 054106, publisher: American Institute of Physics. doi:10.1063/1.3193710.
URL http://aip.scitation.org/doi/full/10.1063/1.3193710

[8] A. J. W. Thom, Stochastic Coupled Cluster Theory, Physical Review Letters 105 (26) (2010) 263004, publisher: American Physical Society. doi:10.1103/PhysRevLett.105.263004.
URL https://link.aps.org/doi/10.1103/PhysRevLett.105.263004

[9] N. S. Blunt, T. W. Rogers, J. S. Spencer, W. M. C. Foulkes, Density-matrix quantum Monte Carlo method, Physical Review B 89 (24) (2014) 245124, publisher: American Physical Society. doi:10.1103/PhysRevB.89.245124.
URL https://link.aps.org/doi/10.1103/PhysRevB.89.245124

[10] J. S. Spencer, N. S. Blunt, W. M. Foulkes, The sign problem and population dynamics in the full configuration interaction quantum Monte Carlo method, The Journal of Chemical Physics 136 (5) (2012) 054110, publisher: American Institute of Physics. doi:10.1063/1.3681396.
URL http://aip.scitation.org/doi/10.1063/1.3681396

[11] J. S. Spencer, N. S. Blunt, S. Choi, J. Etrych, M.-A. Filip, W. M. C. Foulkes, R. S. T. Franklin, W. J. Handley, F. D. Malone, V. A. Neufeld, R. Di Remigio, T. W. Rogers, C. J. C. Scott, J. J. Shepherd, W. A. Vigor, J. Weston, R. Xu, A. J. W. Thom, The HANDE-QMC Project: Open-Source Stochastic Quantum Chemistry from the Ground State Up, Journal of Chemical Theory and Computation 15 (3) (2019) 1728–1742, publisher: American Chemical Society. doi:10.1021/acs.jctc.8b01217.
URL https://doi.org/10.1021/acs.jctc.8b01217

[12] T. Helgaker, P. Jorgensen, J. Olsen, Molecular electronic-structure theory, John Wiley & Sons, 2014.

[13] W. Kohn, Nobel Lecture: Electronic structure of matter—wave functions and density functionals, Reviews of Modern Physics 71 (5) (1999) 1253–1266, publisher: American Physical Society. doi:10.1103/RevModPhys.71.1253.
URL https://link.aps.org/doi/10.1103/RevModPhys.71.1253

[14] P. J. Knowles, N. C. Handy, A determinant based full configuration interaction program, Computer Physics Communications 54 (1) (1989) 75–83. doi:10.1016/0010-4655(89)90033-7.
URL https://www.sciencedirect.com/science/article/pii/0010465589900337

[15] J. Olsen, B. O. Roos, P. Jo/rgensen, H. J. A. Jensen, Determinant based configuration interaction algorithms for complete and restricted configuration interaction spaces, The Journal of Chemical Physics 89 (4) (1988) 2185–2192, publisher: American Institute of Physics. doi:10.1063/1.455063.
URL https://aip.scitation.org/doi/abs/10.1063/1.455063

[16] C. David Sherrill, H. F. Schaefer, The Configuration Interaction Method: Advances in Highly Correlated Approaches, in: P.-O. Löwdin, J. R. Sabin, M. C. Zerner, E. Brändas (Eds.), Advances in Quantum Chemistry, Vol. 34, Academic Press, 1999, pp. 143–269. doi:10.1016/S0065-3276(08)60532-8.
URL https://www.sciencedirect.com/science/article/pii/S0065327608605328

[17] E. Rossi, G. L. Bendazzoli, S. Evangelisti, D. Maynau, A full-configuration benchmark for the N2 molecule, Chemical Physics Letters 310 (5) (1999) 530–536. doi:10.1016/S0009-2614(99)00791-5.
URL https://www.sciencedirect.com/science/article/pii/S0009261499007915

[18] Z. Gan, D. J. Grant, R. J. Harrison, D. A. Dixon, The lowest energy states of the group-IIIA–group-VA heteronuclear diatomics: BN, BP, AlN, and AlP from full configuration interaction calculations, The Journal of Chemical Physics 125 (12) (2006) 124311, publisher: American Institute of Physics. doi:10.1063/1.2335446.
URL https://aip.scitation.org/doi/10.1063/1.2335446

[19] K. D. Vogiatzis, D. Ma, J. Olsen, L. Gagliardi, W. A. de Jong, Pushing configuration-interaction to the limit: Towards massively parallel MCSCF calculations, The Journal of Chemical Physics 147 (18) (2017) 184111, publisher: American Institute of Physics. doi:10.1063/1.4989858.
URL https://aip.scitation.org/doi/10.1063/1.4989858

[20] L. S. Blackford, J. Choi, A. Cleary, E. D'Azevedo, J. Demmel, I. Dhillon, J. Dongarra, S. Hammarling, G. Henry, A. Petitet, K. Stanley, D. Walker, R. C. Whaley, ScaLAPACK Users' Guide, Society for Industrial and Applied Mathematics, Philadelphia, PA, 1997.

[21] C. Lanczos, An iteration method for the solution of the eigenvalue problem of linear differential and integral operators, Jour-

nal of Research of the National Bureau of Standards 45 (4) (1950) 255. doi:10.6028/jres.045.026.
URL https://nvlpubs.nist.gov/nistpubs/jres/045/jresv45n4p255_A1b.pdf

[22] E. R. Davidson, The iterative calculation of a few of the lowest eigenvalues and corresponding eigenvectors of large real-symmetric matrices, Journal of Computational Physics 17 (1) (1975) 87–94. doi:10.1016/0021-9991(75)90065-0.
URL https://www.sciencedirect.com/science/article/pii/0021999175900650

[23] M. Crouzeix, B. Philippe, M. Sadkane, The Davidson Method, SIAM Journal on Scientific Computing 15 (1) (1994) 62–76, publisher: Society for Industrial and Applied Mathematics. doi:10.1137/0915004.
URL https://epubs.siam.org/doi/abs/10.1137/0915004

[24] M. L. Leininger, C. D. Sherrill, W. D. Allen, H. F. Schaefer III, Systematic Study of Selected Diagonalization Methods for Configuration Interaction Matrices, Journal of Computational Chemistry 22 (13) (2001) 1574–1589, _eprint: https://onlinelibrary.wiley.com/doi/pdf/10.1002/jcc.1111. doi:10.1002/jcc.1111.
URL https://onlinelibrary.wiley.com/doi/abs/10.1002/jcc.1111

[25] A. S. Householder, Unitary Triangularization of a Nonsymmetric Matrix, Journal of the ACM 5 (4) (1958) 339–342. doi:10.1145/320941.320947.
URL https://dl.acm.org/doi/10.1145/320941.320947

[26] A. Stathopoulos, Y. Saad, K. Wu, Dynamic Thick Restarting of the Davidson, and the Implicitly Restarted Arnoldi Methods, SIAM Journal on Scientific Computing 19 (1) (1998) 227–245, publisher: Society for Industrial and Applied Mathematics. doi:10.1137/S1064827596304162.
URL https://epubs.siam.org/doi/abs/10.1137/S1064827596304162

[27] J. S. Spencer, A. J. W. Thom, Developments in stochastic coupled cluster theory: The initiator approximation and application to the uniform electron gas, The Journal of Chemical Physics 144 (8) (2016) 084108, publisher: American Institute of Physics. doi:10.1063/1.4942173.
URL http://aip.scitation.org/doi/full/10.1063/1.4942173

[28] I. Shavitt, R. J. Bartlett, Many-Body Methods in Chemistry and Physics: MBPT and Coupled-Cluster Theory, Cambridge Molecular Science, Cambridge University Press, Cambridge, 2009. doi:10.1017/CBO9780511596834.
URL https://www.cambridge.org/core/books/manybody-methods-in-chemistry-and-physics/D12027E4DAF75CE8214671D842C6B80C

[29] H. Flyvbjerg, H. G. Petersen, Error estimates on averages of correlated data, The Journal of Chemical Physics 91 (1) (1989) 461–466, publisher: American Institute of Physics. doi:10.1063/1.457480.
URL https://aip.scitation.org/doi/10.1063/1.457480

[30] T. Ichibha, K. Hongo, R. Maezono, A. J. W. Thom, Making the most of data: Quantum Monte Carlo Post-Analysis Revisited, arXiv:1904.09934 [physics]ArXiv: 1904.09934 (Apr. 2019).
URL http://arxiv.org/abs/1904.09934

[31] K. Guther, R. J. Anderson, N. S. Blunt, N. A. Bogdanov, D. Cleland, N. Dattani, W. Dobrautz, K. Ghanem, P. Jeszenszki, N. Liebermann, G. L. Manni, A. Y. Lozovoi, H. Luo, D. Ma, F. Merz, C. Overy, M. Rampp, P. K. Samanta, L. R. Schwarz, J. J. Shepherd, S. D. Smart, E. Vitale, O. Weser, G. H. Booth, A. Alavi, NECI: N-Electron Configuration Interaction with an emphasis on state-of-the-art stochastic methods, The Journal of Chemical Physics 153 (3) (2020) 034107, publisher: American Institute of Physics. doi:10.1063/5.0005754.
URL http://aip.scitation.org/doi/full/10.1063/5.0005754

[32] D. Cleland, G. H. Booth, A. Alavi, Communications: Survival of the fittest: Accelerating convergence in full configuration-interaction quantum Monte Carlo, The Journal of Chemical Physics 132 (4) (2010) 041103, publisher: American Institute of Physics. doi:10.1063/1.3302277.
URL http://aip.scitation.org/doi/10.1063/1.3302277

[33] N. S. Blunt, Communication: An efficient and accurate perturbative correction to initiator full configuration interaction quantum Monte Carlo, The Journal of Chemical Physics 148 (22) (2018) 221101, publisher: American Institute of Physics. doi:10.1063/1.5037923.
URL http://aip.scitation.org/doi/full/10.1063/1.5037923

[34] V. A. Neufeld, A. J. W. Thom, Accelerating Convergence in Fock Space Quantum Monte Carlo Methods, Journal of Chemical Theory and Computation 16 (3) (2020) 1503–1510, publisher: American Chemical Society. doi:10.1021/acs.jctc.9b01023.
URL https://doi.org/10.1021/acs.jctc.9b01023

[35] N. S. Blunt, A. J. W. Thom, C. J. C. Scott, Preconditioning and Perturbative Estimators in Full Configuration Interaction Quantum Monte Carlo, Journal of Chemical Theory and Computation 15 (6) (2019) 3537–3551, publisher: American Chemical Society. doi:10.1021/acs.jctc.9b00049.
URL https://doi.org/10.1021/acs.jctc.9b00049

[36] G. H. Booth, S. D. Smart, A. Alavi, Linear-scaling and parallelisable algorithms for stochastic quantum chemistry, Molecular Physics 112 (14) (2014) 1855–1869, publisher: Taylor & Francis _eprint: https://doi.org/10.1080/00268976.2013.877165. doi:10.1080/00268976.2013.877165.
URL https://doi.org/10.1080/00268976.2013.877165

[37] A. A. Holmes, H. J. Changlani, C. J. Umrigar, Efficient Heat-Bath Sampling in Fock Space, Journal of Chemical Theory and Computation 12 (4) (2016) 1561–1571, publisher: American Chemical Society. doi:10.1021/acs.jctc.5b01170.
URL https://doi.org/10.1021/acs.jctc.5b01170

[38] V. A. Neufeld, A. J. W. Thom, Exciting Determinants in Quantum Monte Carlo: Loading the Dice with Fast, Low-Memory Weights, Journal of Chemical Theory and Computation 15 (1) (2019) 127–140, publisher: American Chemical Society. doi:10.1021/acs.jctc.8b00844.
URL https://doi.org/10.1021/acs.jctc.8b00844

[39] J. D. Power, R. M. Pitzer, Inequalities For Electron Repulsion Integrals, Chemical Physics Letters 24 (4) (1974) 478–483. doi:10.1016/0009-2614(74)80159-4.
URL https://www.sciencedirect.com/science/article/pii/0009261474801594

[40] C. J. C. Scott, A. J. W. Thom, Stochastic coupled cluster theory: Efficient sampling of the coupled cluster expansion, The Journal of Chemical Physics 147 (12) (2017) 124105, publisher: American Institute of Physics. doi:10.1063/1.4991795.
URL http://aip.scitation.org/doi/full/10.1063/1.4991795

[41] G. Giuliani, G. Vignale, Quantum Theory of the Electron Liquid, Cambridge University Press, 2005. doi:10.1017/CBO9780511619915.

[42] R. M. Martin, Electronic Structure: Basic Theory and Practical

Methods, Cambridge University Press, 2004. doi:10.1017/CBO9780511805769.

[43] P.-F. Loos, P. M. W. Gill, The uniform electron gas, WIREs Computational Molecular Science 6 (4) (2016) 410–429, _eprint: https://onlinelibrary.wiley.com/doi/pdf/10.1002/wcms.1257. doi:10.1002/wcms.1257.
URL https://onlinelibrary.wiley.com/doi/abs/10.1002/wcms.1257

[44] R. D. Mattuck, A guide to Feynman diagrams in the many-body problem, Courier Corporation, 1992.

[45] A. L. Fetter, J. D. Walecka, Quantum theory of many-particle systems, Courier Corporation, 2012.

[46] L. M. Fraser, W. M. C. Foulkes, G. Rajagopal, R. J. Needs, S. D. Kenny, A. J. Williamson, Finite-size effects and Coulomb interactions in quantum Monte Carlo calculations for homogeneous systems with periodic boundary conditions, Physical Review B 53 (4) (1996) 1814–1832, publisher: American Physical Society. doi:10.1103/PhysRevB.53.1814.
URL https://link.aps.org/doi/10.1103/PhysRevB.53.1814

[47] T. Schoof, S. Groth, J. Vorberger, M. Bonitz, Ab Initio Thermodynamic Results for the Degenerate Electron Gas at Finite Temperature, Physical Review Letters 115 (13) (2015) 130402, publisher: American Physical Society. doi:10.1103/PhysRevLett.115.130402.
URL https://link.aps.org/doi/10.1103/PhysRevLett.115.130402

[48] J. J. Shepherd, A. Grüneis, G. H. Booth, G. Kresse, A. Alavi, Convergence of many-body wave-function expansions using a plane-wave basis: From homogeneous electron gas to solid state systems, Physical Review B 86 (3) (2012) 035111, publisher: American Physical Society. doi:10.1103/PhysRevB.86.035111.
URL https://link.aps.org/doi/10.1103/PhysRevB.86.035111

[49] D. M. Ceperley, B. J. Alder, Ground State of the Electron Gas by a Stochastic Method, Physical Review Letters 45 (7) (1980) 566–569, publisher: American Physical Society. doi:10.1103/PhysRevLett.45.566.
URL https://link.aps.org/doi/10.1103/PhysRevLett.45.566

[50] F. H. Zong, C. Lin, D. M. Ceperley, Spin polarization of the low-density three-dimensional electron gas, Physical Review E 66 (3) (2002) 036703, publisher: American Physical Society. doi:10.1103/PhysRevE.66.036703.
URL https://link.aps.org/doi/10.1103/PhysRevE.66.036703

[51] N. D. Drummond, Z. Radnai, J. R. Trail, M. D. Towler, R. J. Needs, Diffusion quantum Monte Carlo study of three-dimensional Wigner crystals, Physical Review B 69 (8) (2004) 085116, publisher: American Physical Society. doi:10.1103/PhysRevB.69.085116.
URL https://link.aps.org/doi/10.1103/PhysRevB.69.085116

[52] S. H. Vosko, L. Wilk, M. Nusair, Accurate spin-dependent electron liquid correlation energies for local spin density calculations: a critical analysis, Canadian Journal of Physics 58 (8) (1980) 1200–1211. doi:10.1139/p80-159.
URL http://www.nrcresearchpress.com/doi/10.1139/p80-159

[53] J. P. Perdew, Y. Wang, Accurate and simple analytic representation of the electron-gas correlation energy, Physical Review B 45 (23) (1992) 13244–13249, publisher: American Physical Society. doi:10.1103/PhysRevB.45.13244.
URL https://link.aps.org/doi/10.1103/PhysRevB.45.13244

[54] R. F. Bishop, K. H. Lührmann, Electron correlations: I. Ground-state results in the high-density regime, Physical Review B 17 (10) (1978) 3757–3780, publisher: American Physical Society. doi:10.1103/PhysRevB.17.3757.
URL https://link.aps.org/doi/10.1103/PhysRevB.17.3757

[55] R. F. Bishop, K. H. Lührmann, Electron correlations. II. Ground-state results at low and metallic densities, Physical Review B 26 (10) (1982) 5523–5557, publisher: American Physical Society. doi:10.1103/PhysRevB.26.5523.
URL https://link.aps.org/doi/10.1103/PhysRevB.26.5523

[56] J. J. Shepherd, T. M. Henderson, G. E. Scuseria, Range-Separated Brueckner Coupled Cluster Doubles Theory, Physical Review Letters 112 (13) (2014) 133002, publisher: American Physical Society. doi:10.1103/PhysRevLett.112.133002.
URL https://link.aps.org/doi/10.1103/PhysRevLett.112.133002

[57] V. A. Neufeld, A. J. W. Thom, A study of the dense uniform electron gas with high orders of coupled cluster, The Journal of Chemical Physics 147 (19) (2017) 194105, publisher: American Institute of Physics. doi:10.1063/1.5003794.
URL http://aip.scitation.org/doi/10.1063/1.5003794

[58] Z. Xianyi, W. Qian, Z. Yunquan, Model-driven Level 3 BLAS Performance Optimization on Loongson 3A Processor, in: 2012 IEEE 18th International Conference on Parallel and Distributed Systems, 2012, pp. 684–691, iSSN: 1521-9097. doi:10.1109/ICPADS.2012.97.

[59] F. Jensen, Introduction to computational chemistry, John wiley & sons, 2017.

[60] T. H. Dunning, Gaussian basis sets for use in correlated molecular calculations. I. The atoms boron through neon and hydrogen, The Journal of Chemical Physics 90 (2) (1989) 1007–1023, publisher: American Institute of Physics. doi:10.1063/1.456153.
URL http://aip.scitation.org/doi/10.1063/1.456153

[61] R. Ditchfield, W. J. Hehre, J. A. Pople, Self-Consistent Molecular-Orbital Methods. IX. An Extended Gaussian-Type Basis for Molecular-Orbital Studies of Organic Molecules, The Journal of Chemical Physics 54 (2) (1971) 724–728, publisher: American Institute of Physics. doi:10.1063/1.1674902.
URL http://aip.scitation.org/doi/10.1063/1.1674902

[62] A. Schäfer, H. Horn, R. Ahlrichs, Fully optimized contracted Gaussian basis sets for atoms Li to Kr, The Journal of Chemical Physics 97 (4) (1992) 2571–2577, publisher: American Institute of Physics. doi:10.1063/1.463096.
URL http://aip.scitation.org/doi/abs/10.1063/1.463096

[63] A. Schäfer, C. Huber, R. Ahlrichs, Fully optimized contracted Gaussian basis sets of triple zeta valence quality for atoms Li to Kr, The Journal of Chemical Physics 100 (8) (1994) 5829–5835, publisher: American Institute of Physics. doi:10.1063/1.467146.
URL http://aip.scitation.org/doi/abs/10.1063/1.467146

[64] L. A. Curtiss, P. C. Redfern, K. Raghavachari, Gaussian-4 theory using reduced order perturbation theory, The Journal of Chemical Physics 127 (12) (2007) 124105, publisher: American Institute of Physics. doi:10.1063/1.2770701.
URL http://aip.scitation.org/doi/full/10.1063/1.2770701

[65] A. Karton, E. Rabinovich, J. M. L. Martin, B. Ruscic, W4 theory for computational thermochemistry: In pursuit of confident sub-kJ/mol predictions, The Journal of Chemical Physics 125 (14) (2006) 144108, publisher: American Institute of Physics. doi:10.1063/1.2348881.
URL http://aip.scitation.org/doi/full/10.1063/1.2348881

[66] N. J. DeYonker, T. R. Cundari, A. K. Wilson, The correlation consistent composite approach (ccCA): An alternative to the Gaussian-n methods, The Journal of Chemical Physics 124 (11) (2006) 114104, publisher: American Institute of Physics. doi:10.1063/1.2173988.
URL http://aip.scitation.org/doi/full/10.1063/1.2173988

[67] T. N. Mihm, B. Yang, J. J. Shepherd, Power Laws Used to Extrapolate the Coupled Cluster Correlation Energy to the Thermodynamic Limit, Journal of Chemical Theory and Computation 17 (5) (2021) 2752–2758, publisher: American Chemical Society. doi:10.1021/acs.jctc.0c01171.
URL https://doi.org/10.1021/acs.jctc.0c01171

[68] P. Virtanen, R. Gommers, T. E. Oliphant, M. Haberland, T. Reddy, D. Cournapeau, E. Burovski, P. Peterson, W. Weckesser, J. Bright, S. J. van der Walt, M. Brett, J. Wilson, K. J. Millman, N. Mayorov, A. R. J. Nelson, E. Jones, R. Kern, E. Larson, C. J. Carey, l. Polat, Y. Feng, E. W. Moore, J. VanderPlas, D. Laxalde, J. Perktold, R. Cimrman, I. Henriksen, E. A. Quintero, C. R. Harris, A. M. Archibald, A. H. Ribeiro, F. Pedregosa, P. van Mulbregt, SciPy 1.0: fundamental algorithms for scientific computing in Python, Nature Methods 17 (3) (2020) 261–272, number: 3 Publisher: Nature Publishing Group. doi:10.1038/s41592-019-0686-2.
URL http://www.nature.com/articles/s41592-019-0686-2

[69] J. J. Shepherd, G. H. Booth, A. Alavi, Investigation of the full configuration interaction quantum Monte Carlo method using homogeneous electron gas models, The Journal of Chemical Physics 136 (24) (2012) 244101, publisher: American Institute of Physics. doi:10.1063/1.4720076.
URL https://aip.scitation.org/doi/10.1063/1.4720076

[70] T. pandas development team, pandas-dev/pandas: Pandas (Feb. 2020). doi:10.5281/zenodo.3509134.
URL https://doi.org/10.5281/zenodo.3509134

[71] T. Zhang, F. A. Evangelista, A Deterministic Projector Configuration Interaction Approach for the Ground State of Quantum Many-Body Systems, Journal of Chemical Theory and Computation 12 (9) (2016) 4326–4337, publisher: American Chemical Society. doi:10.1021/acs.jctc.6b00639.
URL https://doi.org/10.1021/acs.jctc.6b00639